International Journal of Biological Macromolecules 199 (2022) 108–120

Contents lists available at ScienceDirect

International Journal of Biological Macromolecules

journal homepage: www.elsevier.com/locate/ijbiomac

Improvement of salicylic acid biological effect through its encapsulation with silica or chitosan

Jimmy Sampedro-Guerrero [a], Vicente Vives-Peris [a], Aurelio Gomez-Cadenas [a,*], Carolina Clausell-Terol [b,*]

[a] Departamento de Ciencias Agrarias y del Medio Natural, Universitat Jaume I, 12071 Castellón, Spain
[b] Departamento de Ingeniería Química, Instituto Universitario de Tecnología Cerámica, Universitat Jaume I, 12071 Castellón, Spain

ARTICLE INFO

Keywords:
Antifungal activity
Arabidopsis
Root growth

ABSTRACT

Attacks of necrotrophic and biotrophic fungi affect a large number of crops worldwide and are difficult to control with fungicides due to their genetic plasticity. Encapsulation technology is a good alternative for controlling fungal diseases. In this work, encapsulated samples of salicylic acid (SA) with silica (Si:SA) or chitosan (Ch:SA) at three different ratios were prepared by spray drying, and morphological and physicochemical characterised. Therefore, size distribution, specific surface area, thermal stability, encapsulation efficiency, and in-vitro SA release were determined. Biological activity of encapsulated samples were tested against different fungi of agricultural interest at various concentrations (0–1000 μM). Treatments prepared with the lowest ratios for both capsules, were found to have the best antifungal effect in an in vitro system, inhibiting the mycelial growth of Alternaria alternata, Botrytis cinerea, Fusarium oxysporum and Geotrichum candidum. Similarly, treatments with the lowest ratios of both encapsulated samples reduced free SA toxicity on Arabidopsis thaliana seeds. In this system, plants treated with capsules had higher root and rosette development than those treated with free SA. In conclusion, a product with a great potential in agriculture that shows high antifungal capacity and low toxicity for plants have been developed through a controlled and industrially viable process.

1. Introduction

Every year, pathogenic fungi affect leaves, roots, and seeds of important crops causing significant effects and losses in agriculture [1]. The abusive use of chemical fungicides to control fungal diseases in plants has decreased their effectiveness and caused environmental hazards that increase progressively.

Furthermore, the uncontrolled use of these chemical agents have caused the development of fungi resistances [2]. Due to the large number of affected crops, chemical-biological alternatives have recently been applied to control different pathogens and mitigate several environmental stresses. Plants produce natural compounds named phytohormones that control their vegetative growth, floral development, fruit growth and maturation and senescence, among others. Moreover, they act by forming complex phytohormone networks that control and balance plant stress responses, and protect them against several pathogens [3]. Phytohormones can be synthetically produced and then are called Plant Growth Regulators (PGRs) [4]. This group of compounds includes auxins, cytokinins, gibberellins, jasmonic acid, abscisic acid and salicylic acid (SA) [5]. PGRs are widely used in several areas of agriculture to increase the production of crops with better phytosanitary and commercial characteristics [6].

The phenolic ring linked to a hydroxyl group in the SA structure has a vital role on the regulation of crucial processes of plants, such as seed germination, photosynthesis, redox homeostasis, senescence and vegetative growth [7]. SA can be present in the form of a free fraction or in a glycosylated/glucose-ester/methylated conjugate form, and it can be synthesized by two different and compartmentalized routes [8]. In the first one, denominated the phenylalanine route, phenylalanine (Phe) is converted to *trans*-cinnamic acid (t-CA), then t-CA gets oxidized to benzoic acid (BA) and, finally, the aromatic ring of BA is hydroxyled to form SA. On the other route, called the isochorismate route, chorismate is initially transformed in isochorismate (IC) and then in SA [9]. Several studies reveal that SA regulates many tolerance responses to abiotic stress [10,11]; moreover, when seeds are imbibed in SA or it is applied as a foliar treatment through exogenous application, it can control

* Corresponding authors.
E-mail address: cclausel@uji.es (C. Clausell-Terol).

https://doi.org/10.1016/j.ijbiomac.2021.12.124
Received 23 September 2021; Received in revised form 9 December 2021; Accepted 19 December 2021
Available online 30 December 2021

pathogenic diseases and enhance the plant development [12]. The main problem with the exogenous application of SA is to achieve a prolonged and sustained effect, given its easy degradation when exposed to light or significant temperature changes, which can result in a decrease in efficiency and/or loss of activity [13].

Encapsulation is used for coating active agents with protective materials, improving their stability and activity, and even reducing environmental impacts [14,15]. Capsules are generally nanomaterials, used as delivery systems for the encapsulation of different active agents, such as enzymes, proteins, genes, metabolites, hormones, among others. The surface of the capsule increases the bioavailability and solubility of the active molecules, and the small size that they usually present facilitates the encapsulation process and increases the release of the active molecules by increasing the specific and contact surface [16]. Additionally, capsules are used for their biocompatibility, controlled and targeted release, and chemical stability [17].

Drug carriers include polysaccharides such as chitosan, which is a natural polymer with useful biocompatibility characteristics, non-toxicity effects and excellent biodegradability. Polysaccharides are an ideal choice as delayed release agents due to their abundance in nature, structural stability, and inexpensiveness [18], which explains the different applications of chitosan carrier systems in crop protection[19]. Like chitosan, silica allows the encapsulation of functional components such as drugs, fluorescent materials and pigments, which are mainly used in drug delivery, imaging and sensing technologies [20]. Silica capsules, with a core–shell hierarchical structure, have recently generated interest as a low-cost and environmental friendly encapsulation technology with short time experimentation requirements [21]. Mesoporous silica has been used for encapsulating abscisic acid (ABA) and tested in *Arabidopsis thaliana*, showing an effective prolonged release of ABA and improving the drought resistance of *Arabidopsis* seedlings [22].

The aim of the present work was to obtain bioactive compounds of SA, encapsulated in chitosan or silica particles (at different capsule: active agent ratios) through an easy scalable process at an industrial level, and to study their biological effect on plant growth and anti-pathogenic activity. In addition to the morphology, size and size distribution of the encapsulated samples, their physicochemical characteristics and the hormone release mechanism will be evaluated. Encapsulated samples have a anti-fungal effect greater than free SA, limiting the growth of different fungi. Their effect on *Arabidopsis thaliana* seeds allows deepening on plant growth regulation. The results denote a great potential for applications in agriculture.

2. Materials and methods

2.1. Materials

2.1.1. Raw materials

Chitosan (DG CHI 0.20 g/ml and 85% deacetylated) and pyrogenic amorphous silica (HDK® S13) were purchased from AOXIN (Shanghai, China) and WACKER (Barcelona, Spain), respectively. Salicylic acid (SA), sucrose and tween 80 were purchased from Sigma-Aldrich (St. Louis, USA). Acetone, sodium tripolyphosphate (TPP-Na), European bacteriological and potato dextrose agar (PDA) and petri dishes were purchased from the Spanish companies Labkem, Acrilatos SAU, Condalab and Labkem, respectively. Dichloromethane (DCM) was purchased from Fisher Scientific (Lenexa, USA), tween 20 from PANREAC (Barcelona, Spain), and Myo-Inositol and Murashige & Skoog Medium (Basal Salt Mixture) from Duchefa (Haarlem, The Netherlands).

2.1.2. Fungal and plant materials

Five fungal species (*Alternaria alternata*, *Botrytis cinerea*, *Fusarium oxysporum*, *Geotrichum candidum* and *Phytophthora infestans*) were obtained from the Spanish Type Culture Collection, (Valencia, Spain).

Arabidopsis thaliana wild-type (Col-0) seeds were obtained from the Nottingham Arabidopsis Stock Centre. Seeds were surface sterilized with bleach solution (30% v/v sodium hypochlorite and 0.01 % v/v Tween 20) for 10 min incubation, followed by three washes with distilled sterile water.

2.2. Methods

2.2.1. Preparation of silica and chitosan capsules

Silica encapsulated SA (Si:SA): Three different ratios (see Table 1) were formulated: 1:1, 1:0.5 and 1:0.25. The appropriate amount of SA (according to the ratio) was mixed with 320 ml distilled water by using a planetary mill (Fritsch, Pulverisette®) for 15 min at 120 rpm, using alumina balls as grinding media (~300 g). Amorphous silica was stepwise added and mixed for one hour at 180 rpm.

Chitosan encapsulated SA (Ch:SA): Three different ratios (see Table 1) were prepared (1:1.25, 1:1 and 1:0.5) using the following procedure: 1) 138.6 ml of distilled water and 1.4 ml of acetic acid was planetary mixed for 5 min at 150 rpm to acidify the emulsion, 2) 4.2 g of chitosan was added and planetary mixed for 15 min at 210 rpm, 3) 1.4 ml of tween 80 was added and planetary mixed for 15 min at 210 rpm, 4) the appropriate amount (according to the ratio) of SA and pre-dissolved in dichloromethane (10 min at 500 rpm) was added and planetary mixed for 15 min at 210 rpm, 5) 2.1 g of TPP-Na and 137.9 ml of distilled water was added and planetary mixed for one hour at 210 rpm.

Slurries were maintained in constantly agitation before spray drying. Density was measured in triplicate using 25 ml flasks.

2.2.2. Rheological characterization

The viscosity and rheological behaviour of encapsulated slurries were obtained by conducting tests under steady state conditions using a Bohlin CVO-120 rheometer, controlling the shear stress applied and measuring the shear strain produced. A double gap (DG 40/50) device, composed of two concentric cylinders, was selected to ensure high sensibility with low viscosity suspensions. Initial stirring for 30 s in the rheometer broke up any dispersion inner structure that might have formed, thus eliminating residual history effects. The shear stress was then abruptly reduced to zero. This situation was held for 60 s to enable the dispersion to acquire a controlled, reproducible inner structure. The sequence of the shear test used consisted of an increasing/decreasing logarithmic ramp of shear stress, with twelve pairs of shear rate–shear stress values in each ramp. The samples were thermostated at 25 °C during testing.

2.2.3. Spray drying

Spray drying was performed with a SD-06 spray drier (Lab Plant, UK), with a standard 0.5 mm nozzle. As the liquid was fed to the nozzle with a peristaltic pump, atomization occurred by the force of the compressed air, disrupting the liquid into small droplets. The droplets, together with hot air, were blown into a chamber where the water in the droplets evaporated and discharged out through an exhaust tube. The

Table 1
Characteristics of the encapsulated samples prepared with silica (Si:SA) and chitosan (Ch:SA): Ratio Si/Ch:SA, salicylic acid (SA) and solid content (SC) on the prepared slurries, and encapsulation efficiency (EE) and BET specific surface area (Se) of the encapsulated materials obtained by spray drying.

Sample	Ratio Si/Ch:SA	SA (% w)	SC (% w)	EE (%)	Se (m^2/g)
Si:SA (1:1)	1 : 1	6.8	13.5	63.6 ± 2.9^{ab}	60 ± 3
Si:SA (1:0.5)	1 : 0.5	4.5	13.5	69.4 ± 5.2^{ab}	74 ± 4
Si:SA (1:0.25)	1 : 0.25	2.7	13.5	52.6 ± 4.1^{a}	83 ± 4
Ch:SA (1:1.25)	1 : 1.25	1.7	3.6	46.6 ± 3.9^{ab}	2.3 ± 0.2
Ch:SA (1:1)	1 : 1	1.4	3.4	49.6 ± 1.0^{ab}	2.1 ± 0.2
Ch:SA (1:0.5)	1 : 0.5	0.7	2.8	43.9 ± 3.1^{b}	1.8 ± 0.2

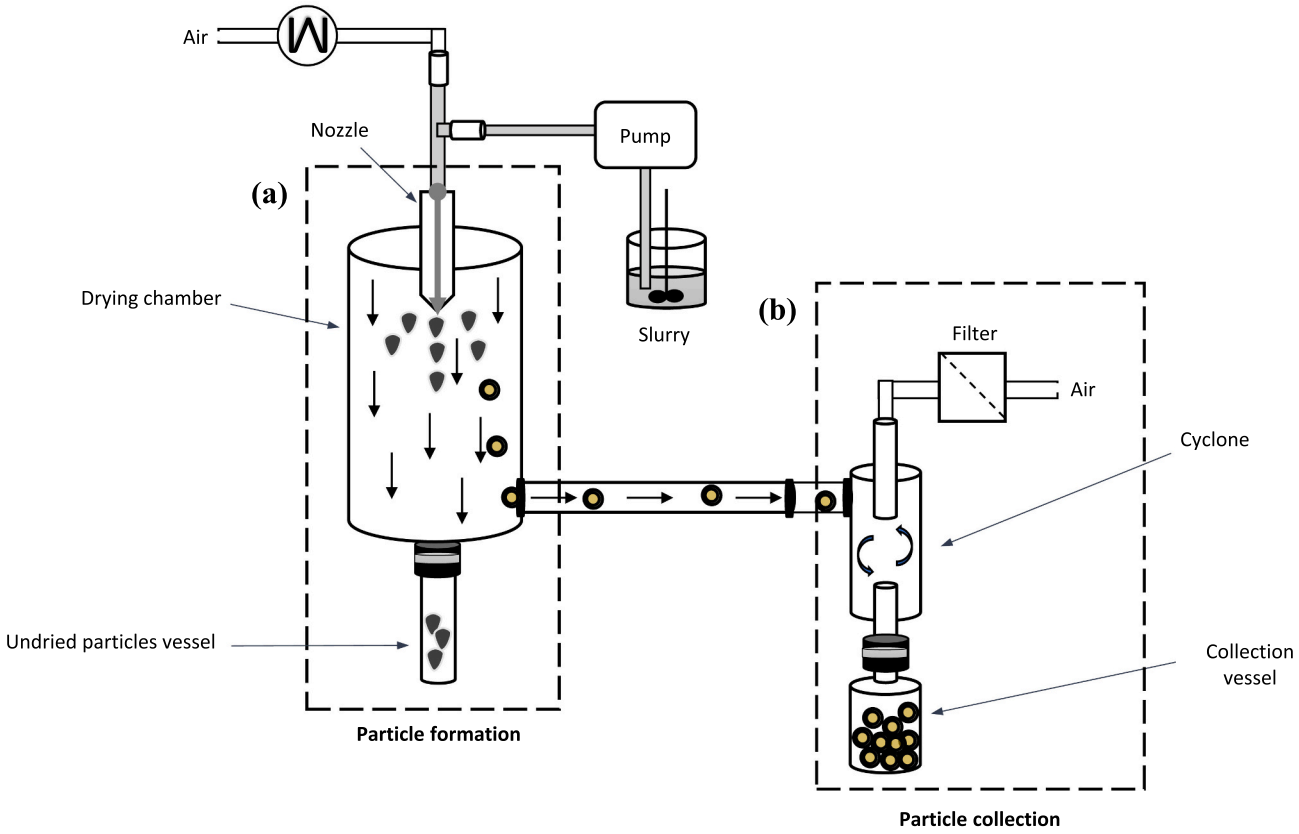

Fig. 1. Schematic diagram of the spray dryer. (a) Encapsulated slurry pumped and particles dried, (b) Recollection of dry particles.

dry product was collected in a collection bottle and stored in plastic bags at room temperature for further characterization. Fig. 1 shows a schematic diagram of the spray drying process.

In the standard condition, the inlet temperature, spray flow, drying air fan and compressed air pressure were set at 150 °C, 10 ml/min, 80% and 1.5 bar, respectively. The drying performance varied from 48 to 79% for the encapsulated slurries prepared with silica (Si:SA) and from 36 to 75% for those prepared with chitosan (Ch:SA).

2.2.4. SEM-EDX

The powdered sample was deposited in a brass sample holder using a conducting carbon adhesive tape and, with a view to favouring conductivity, it was coated with platinum. All the prepared samples were observed and photographed with the backscattered electron and secondary electron signal of a field-emission gun environmental scanning electron microscope (FEG-ESEM) Quattro S of Thermo Fisher.

The backscattered electron signal (CBS detector - All mode) provides information on the topography and composition. The higher the average atomic number of the sample, the more intense is the signal, so that the lightest-coloured areas contain the heaviest elements (composition contrast). The secondary electron signal (ETD detector - SE mode) is more superficial, so that it provides information on the morphology of the sample, highlighting surface irregularities such as cracks, pores, and crystal or grain edges.

Samples were also analysed with an energy-dispersive X-ray microanalysis spectrometer (EDS) connected to the microscope. Note that the electron beam interaction volume is of the order of 3 μm or higher so that, when analysing very small zones, chemical information is received from the surrounding area. It may furthermore be noted that this analysis system detects elements with an atomic number of 6 or higher (from carbon upwards).

2.2.5. Capsule size distribution

Scanning electron microscopic images were used for determining the capsules size distribution. Image processing and analysing was performed with the image analyser software ImageJ. For the characterization of each sample, four images and more than 800 capsules were measured. The capsule area was determined by ¨Analyse particles function¨, and the diameter was calculated assuming that all encapsulated particles were spherical. Capsule size distributions were obtained by representing the accumulated frequency vs diameter.

2.2.6. Encapsulation efficiency (EE)

SA was extracted from both type of capsules, silica and chitosan. Samples were weighed (5–10 mg) and 1.5 ml of 0.1 M HCl was added to each one. After that, the samples were incubated for 24 h at room temperature. Further, capsules were centrifuged at 12500 rpm and supernatant (containing SA) was measured by ultraviolet–visible (UV–vis) spectrophotometric analysis (Thermo Spectronic) at 297 nm. Experiment was realized with three replicates for each ratio of both capsules. EE was calculated by the following equation:

$$EE(\%) = \frac{(TheoreticalSA - DeterminedSA)}{TheoreticalSA} \times 100 \quad (1)$$

where '*Theoretical SA*' is the product of initial mass of the sample (mg) and theoretical SA encapsulated (%) and '*Determined SA*' is the product of SA supernatant concentration (mg/mL) and supernatant reaction volume (mL). SA supernatant concentration was calculated with a calibration curve of free SA.

2.2.7. Specific surface area

Adsorption/desorption curve, using nitrogen gas as adsorbent, was carried out with a Tristar 3000 equipment from Micromeritics, using the Standard ISO9277:1995. Specific surface area was determined according to the BET method using the adsorption isotherm. This parameter

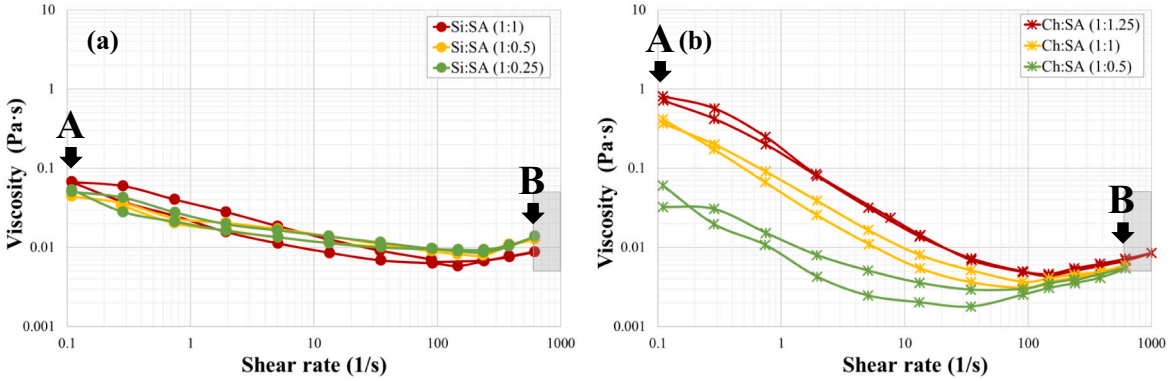

Fig. 2. Viscosity flow behaviour for the encapsulated slurries prepared with silica (a) and chitosan (b) with the three capsule:SA studied ratios. A and B points viscosity values are shown in Table 1. The grey area corresponds to the working area in the atomization process.

was calculated by means of the multipoint method using the following equation:

$$S_{BET}\left(m^2 g^{-1}\right) = n_m \cdot a_{nitrogen} \cdot N_A \quad (2)$$

where n_m is the molar monolayer capacity, $a_{nitrogen}$ is the area of surface occupied by a single adsorbed gas molecule (0.162 nm^2) and N_A is the Avogadro's constant.

The monolayer capacity (nm) was calculated carrying out a linear regression, obtaining the slope and the intercept from the BET equation in which $n_m = (1/(a+b))$, and where a is the slope and b is the intercept. The amount of adsorbed nitrogen was measured by means of a static volumetric method.

Before carrying out the test, sample was dried in an oven at 45 °C for 2 h and, after that it was outgassed with a nitrogen flux at 80 °C for 3 h.

2.2.8. Thermal analysis

Thermogravimetric data were recorded on a Mettler-Toledo, TGA/STDA851e model, which allows simultaneous recording of the weight losses (TG), the derivative (DTG), the differential thermal curves (DTA) and the temperature increases (T), in a dynamic nitrogen atmosphere. Analysis conditions used were maximum temperature 1000 °C, heating rate 10 °C/min and alumina vessel sample holder. The instrument was verified by using different certified reference materials that ensure the traceability of the measurement.

2.2.9. In-vitro SA release

In vitro release study was conducted following the next procedure. The sample (10 mg) was mixed with 2 ml distilled sterile water. The experiment was conducted at pH 7 and room temperature under a constant magnetic stirring of 100 rpm. At specific time intervals (0–24 h), the sample was centrifuged at 12000 rpm for 2 min at 4 °C, and 2 ml supernatant volume was sampled for analysis. Supernatant volume sampled was replaced with an equivalent volume of distilled sterile water in each time tested to keep constant the total volume. The amount of SA released was determined by UV–vis absorption spectroscopy at 297 nm, as described in section 2.2.6. SA release mechanism was evaluated by Korsmeyer-Peppas model [23] using the following equation:

$$\frac{M_t}{M_\infty} = k \cdot t^n \quad (3)$$

where M_t is the amount of SA released at a given time (t), M_∞ is the amount of SA released at infinite time, k is the kinetic constant, and n is the release exponent. From the value of n it is possible to determine whether the release mechanism is Fickian or non-Fickian (anomalous) release. According to the mathematical model, $n < 0.45$ indicates that the system releases the active agent by diffusion, following Fick's law (case I transport); $n > 0.89$ indicates release by relaxation of the polymeric wall or erosion of the particle, case II transport; and $0.45 < n < 0.89$ indicates release by anomalous transport, with both of the aforementioned mechanisms occurring simultaneously [23].

2.2.10. Antifungal activities

Antifungal activity of the capsules was measured by Poison food technique [9]. Different concentrations (100, 500 and 1000 μM) were tested, in quadruple, against five fungal species (see section 2.1.2.). Potato dextrose agar (PDA) medium was mixed with samples and poured in 9 × 15 mm Petri dishes. In the case of fungal species, a 7-days-old mycelial bit (1 × 1 cm) was taken from the peripheral end and placed in the centre of each dish treatment. Following that, dishes were incubated at 25 °C, and the observation of radial mycelial growth was recorded on days 3, 5, 7 and 10. Inhibition rate was calculated by comparing each dish treatment with control at 10 days and using the following equation:

$$Inhibitionrate(\%) = \frac{(Mc - Mt)}{Mc} \times 100 \quad (4)$$

where Mc is the control mycelial growth and Mt is the treatment mycelial growth.

2.2.11. Plant growth and treatment conditions

Seeds were sown in 9 × 15 mm dishes containing Murashige and Skoog medium, 10 g/l sucrose, 100 mg/l myo-inositol, and vitamins [24]. For each treatment, the samples were mixed with the medium and poured in Petri dishes. Seeds were distributed individually in the dishes in two rows with 10 seeds per row. Subsequently, the seeds were stratified for 24 h at 4 °C in the dark to synchronize germination. Dishes were incubated for 0–12 days vertically oriented under long day conditions (16 h of light and 8 h of dark) at 22.5 °C and 60% relative humidity. Treatments consisted of four replicates for each treatment and twenty plants samples for each replicate.

2.2.12. Root development and growth quantification

Petri dishes images were obtained with a scanner (Epson perfection v600 photo) at 600 dpi. The dishes were placed in the scanner with a black surface (included in the scanner) at the top. Different images on days 4, 8 and 12 after sowing were obtained and saved in JPEG format. Size of the roots of each seed were analysed with MyROOT software [25].

2.2.13. Statistical analysis

Statistical analysis was performed with SPSS software version 21. Significant differences among treatment groups were determined by using the Turkey-Kramer HSD test at $p \leq 0.05$. The experiments replicates are detailed in their respective procedure section.

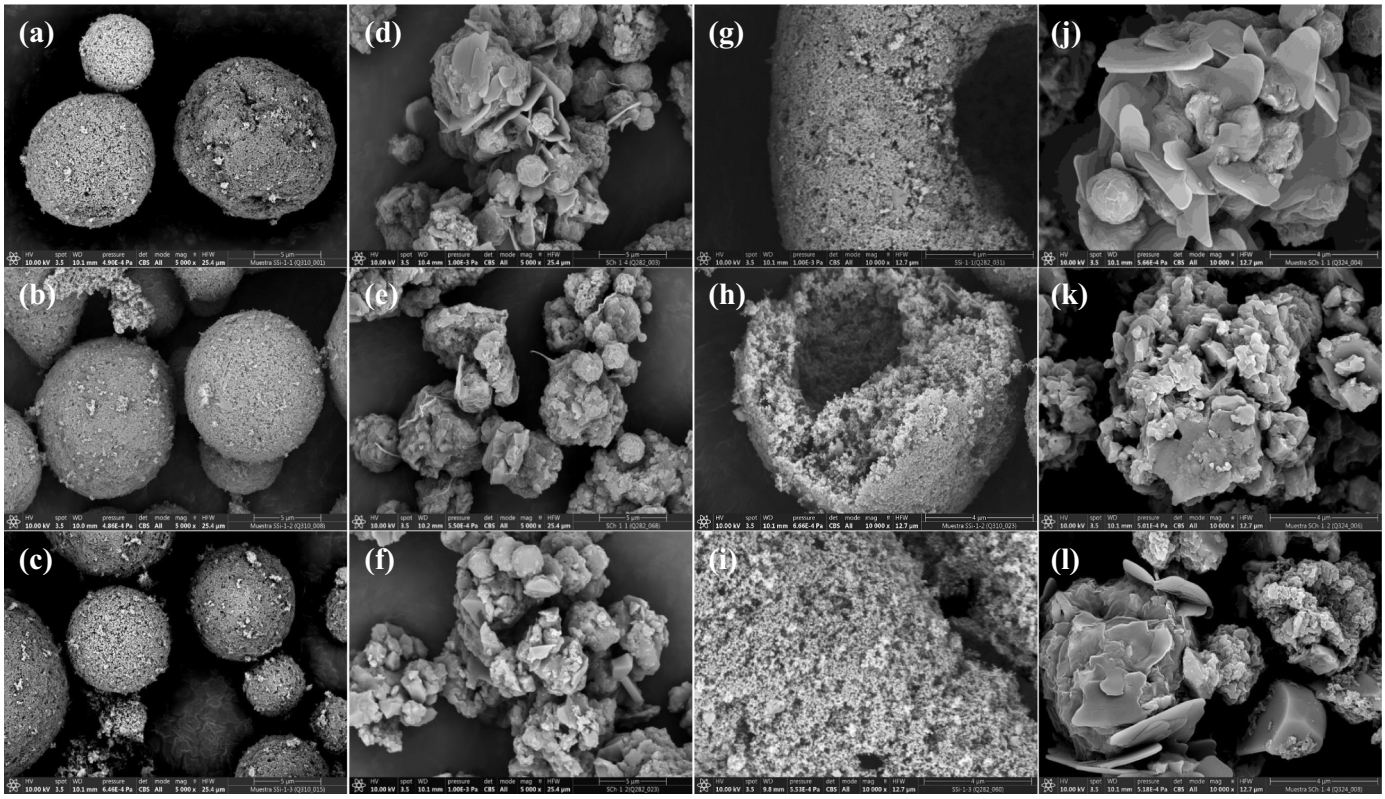

Fig. 3. Scanning electron microscopic (SEM) images of the encapsulated samples prepared with silica (a-b-c-g-h-i) and chitosan (d-e-f-j-k-l) for the three capsule:SA studied ratios. Si:SA (1:1) (a-g), Si:SA (1:0.5) (b-h), Si:SA (1:0.25) (c-i), Ch:SA (1:1.25) (d-j), Ch:SA (1:1) (e-k), Ch:SA (1:0.5) (f-l). (a-b-c-d-e-f) 5000x magnification and (g-h-i-j-k-l) 10000× magnification.

3. Results and discussion

3.1. Formulation and characterization of the encapsulated samples

3.1.1. Rheological characterization

Viscosity measurements at different shear rates are needed to evaluate the suitability of a slurry to be atomized. For a pneumatic atomizer, the shear rate in the slurry increases rapidly as it passes through the nozzle, and once the droplets are formed, the shear rate decreases to zero, and the temperature of the slurry increases to the wet-bulb temperature in the drying chamber, which is considerably lower than the programmed inlet temperature (150 °C in our case) [26].

Fig. 2 shows the rheological behaviour of the encapsulated slurries prepared with silica (Fig. 2a) and chitosan (Fig. 2b), for the three capsule:SA studied ratios. The experiments were conducted over the shear rate range of 0.1–1000 s^{-1} from the upward sweep followed by downward sweep. The viscosity of the slurries at the extremes of the range (points A and B in Fig. 2) are depicted in Supplementary Table 1, together with the density values of the suspensions.

Silica slurries displayed a low shear thinning behaviour, especially given the nanometric nature of the silica particles, which indicates their good dispersion in the slurry. As shown in Fig. 2a, there is no difference between the three studied ratios, probably because all the samples have the same solid content (See Table 1). Silica capsules present a spherical geometry (Fig. 3a-b-c) which makes them symmetrical. Therefore, any option of alignment should be discarded, which explains their low pseudoplasticity.

Chitosan slurries displayed a mild shear thinning behaviour and a differentiated rheological behaviour between ratios (Fig. 2b). The high pseudoplasticity of the chitosan capsules can be explained by their

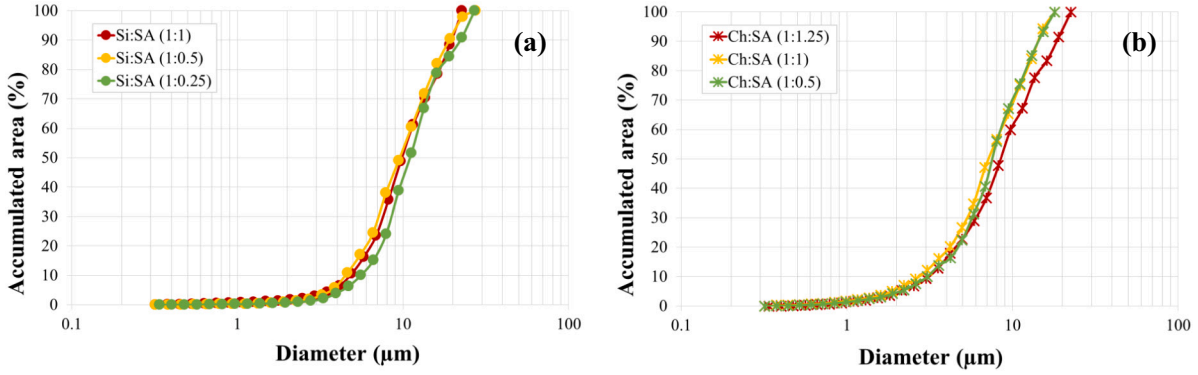

Fig. 4. Capsule size distributions of the samples prepared with silica (a) and chitosan (b) for the three capsule:SA studied ratios. Characteristic diameters (D_{10}, D_{50} and D_{90}) are shown in Table 3.

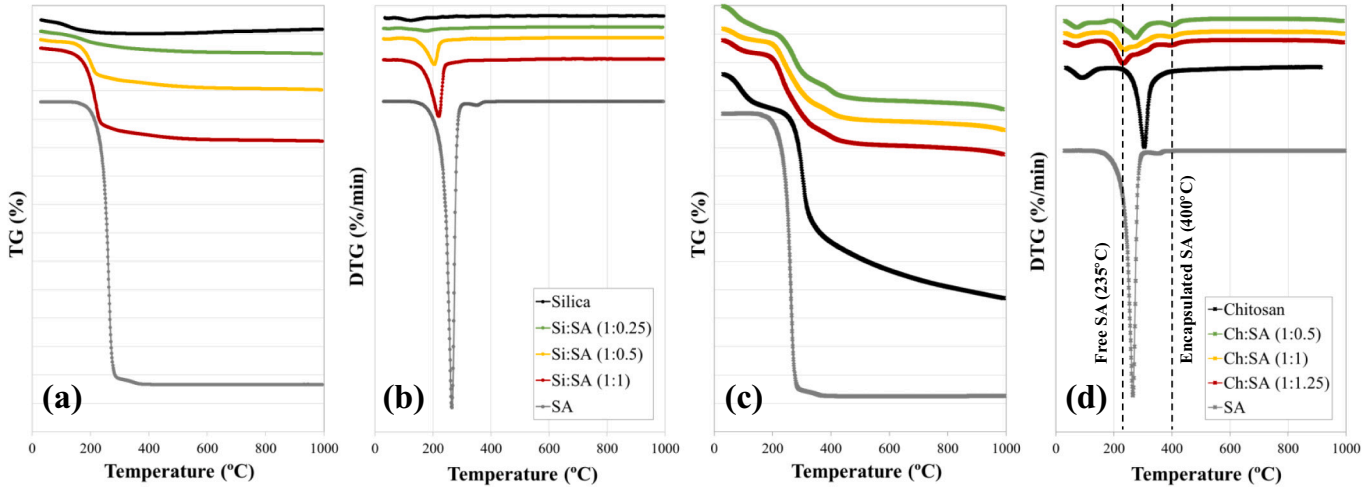

Fig. 5. TG (a, c) and DTG (b, d) curves of the encapsulated samples prepared with silica (a-b) and chitosan (c-d) for the three capsule:SA studied ratios and their corresponding raw materials.

irregular geometry, with the presence of some laminar particles (Fig. 3j-k-l), which can easily align under an external force, decreasing the viscosity of the slurry. The differences observed between ratios are mainly due to the different solid content of the slurries (see Table 1). The higher the SA content, the higher the solid content (due to unavoidable needs of the experimental procedure), increasing the inter-particle network and hence the viscosity of the slurries at low shear rates.

The magnitude of shear thinning i.e. reduction in viscosity with respect to increasing shear rate, reveals information about inter-particle network formation [27]. High shear thinning behaviour means high inter-particle network, which in turn offers more resistance to flow. Accordingly for the purpose of spray drying, it is preferable to have slurries with weak or no inter-particle network [28], with a low viscosity at high shear rates (grey area in Fig. 2a and b) and with a density value lower than 1.4–1.6 g/cm^3. Hence, the prepared silica and chitosan encapsulated SA slurries were found to be suitable to spray drying.

Finally, the difference in the viscosities at any given shear rate gives information about the thixotropy, which can be defined as the property of the slurry that are thick under normal conditions and flows over time when it is stressed. From the rheographs (Fig. 2a and b), it was evident that the thixotropy was negligible, which means that slurries were sufficiently stable and, once again, suitable for the spray drying process [29].

3.1.2. Capsule size distribution

Image analysis of high resolution SEM micrographs allows to determine the size distribution and shape of the capsules [30]. The encapsulated samples with silica (Si:SA) showed a similar spherical shape in the three studied ratios (see Fig. 3a-b-c) and a highly porous structure (characteristic of the amorphous silica capsules) where the incorporation of the hormone occurs without altering the structure of the capsule itself (see Fig. 3g-h-i). The encapsulated samples with chitosan (Ch:SA) showed an irregular non-spherical shape in the three studied ratios (see Fig. 4d-e-f-j-k-l). This suggests that, contrary to Si:SA samples (where SA is embedded into the capsule material [31]), SA should be entrapped within chitosan particles. The chitosan chains will subsequently cross-link with TPP-Na, resulting in a aggregated linkage formation [32,33].

SEM micrographs analyses were conducted by ImageJ software, calculating the diameter of individual capsules of each sample using the threshold option, and estimating the area values assuming a spherical geometry. Capsule size distribution curves were obtained by representing diameter values vs accumulated area (see Fig. 4a and b for Si:SA and Ch:SA samples, respectively). D_{90}, D_{50} and D_{10} equivalent diameters were determined from the curves and depicted in Supplementary Table 2. Equivalent diameters designated as D_{10}, D_{50}, and D_{90} indicate that 10%, 50%, and 90% of capsules are smaller than such values. As shown in Fig. 4 and Supplementary Table 2, the capsule size distributions of all samples were quite similar, with a D_{50} value of 9.6–11.0 mm for the encapsulated samples with silica (Si:SA) and of 7.2–8.5 mm for the ones with chitosan (Ch:SA).

An important factor to consider is the toxicity of the samples when applied to living organisms. Certain size values could increase its toxicity by modifying the characteristics of the surface of the samples and the free energy, enhancing the potential catalytic surface to carry out the chemical reactions between the biological components and the surface of the particles [34]. While the level of toxicity of many materials is well known, it is still unknown how concentration, particle size or particle size distribution can promote new toxicological effects [35]. Therefore, it is important to note that, in our case, all samples have a similar capsule size and capsule size distribution, so no differences in toxicity can be expected for this reason[36,37].

3.1.3. Thermal analysis

To assess thermal stability of capsules, thermogravimetric analysis was used. The decomposition temperature (T_d) is the temperature corresponding to the maximum mass loss, which is clearly observed as a peak when the rate of mass loss versus temperature, a so-called DTG thermogram, is plotted [38].

The thermograms of pure and encapsulated materials, for both silica and chitosan, are presented in Fig. 5 (TG-DTG) and in Supplementary Fig. 1 (DTA). Pure silica is thermally quite stable, with a maximum mass loss around 5%. However, pure SA undergone complete endothermic decomposition in one stage at 266 °C, while pure chitosan experienced two reaction stages of thermal decomposition: a first stage at 90 °C (ENDO peak) due to the evaporation of moisture and a second one at 313 °C (EXO peak) which is assigned to the dehydration and decomposition of the material. The ENDO DTA peak of pure SA at 168 °C correspond to SA fusion.

TG-DTG and DTA thermograms of the encapsulated samples (both with silica and chitosan) show an intermediate behaviour compared to the curves of the pure raw materials, confirming the encapsulation process for the three ratios studied for each capsule material. The thermal degradation of the encapsulated samples prepared with silica (Si:SA) (Fig. 5a-b) takes place in one stage, mainly due to the decomposition of the SA, which explains the higher mass loss observed for the higher capsule:SA ratio, that is Si:SA (1:1). Also, SA decomposition rate (observed around 266 °C) decreases for the encapsulated samples, which

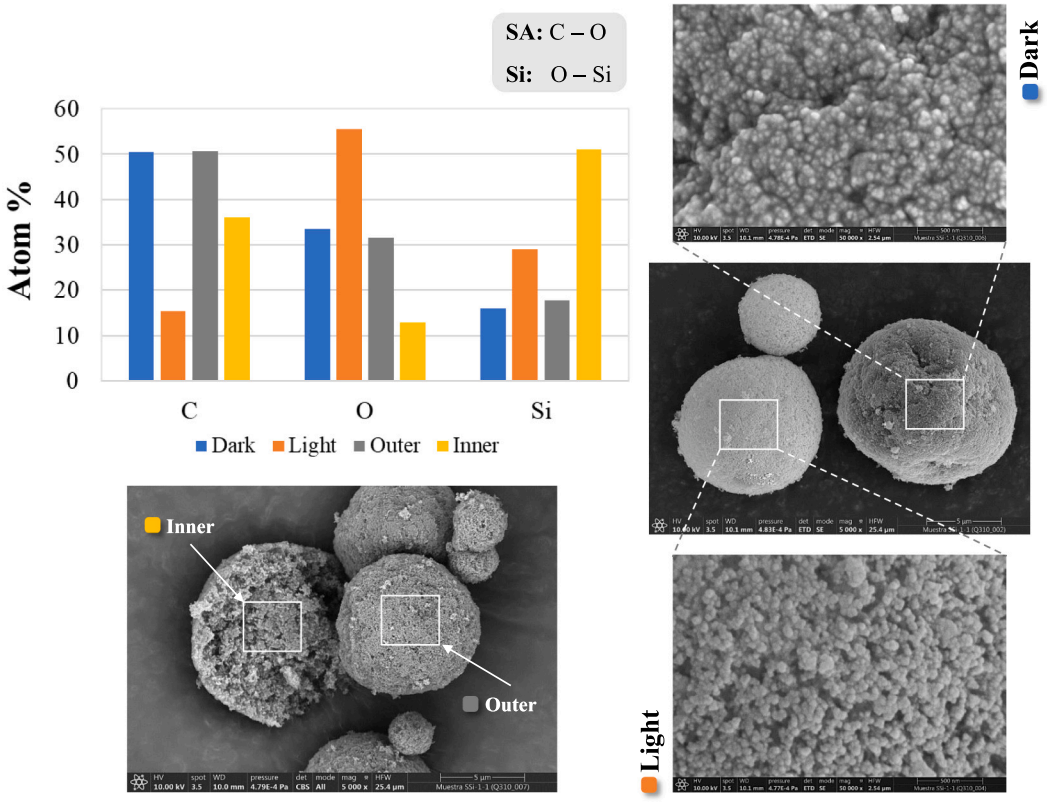

Fig. 6. Semi-quantitative Energy Dispersive X-ray (EDX) microanalysis of the encapsulated samples prepared with silica (Si:SA).

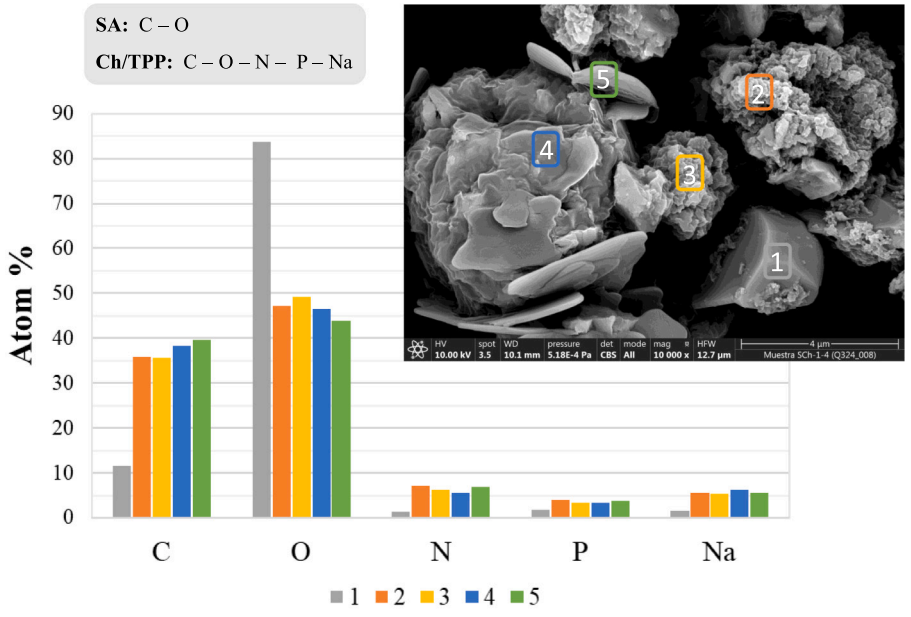

Fig. 7. Semi-quantitative Energy Dispersive X-ray (EDX) microanalysis of the encapsulated samples prepared with chitosan (Ch:SA).

would result in a slower release of SA, compared to free SA.

The thermal degradation of the encapsulated samples prepared with chitosan (Ch:SA) are depicted in Fig. 5c-d. By comparison with the thermogram of the raw materials, the capsules of Ch:SA manifested two new T_d around 200° and 400 °C, which could be ascribed to the loss of free SA and encapsulated SA, respectively. The result, which is in agreement with previous studies from oils of different nature [33,38], reveals the achievement of SA loading into chitosan particles. It should be pointed out that the encapsulated SA decomposed at higher temperature than free SA, reflecting the improved thermal stability of SA by encapsulation. However, the T_d of free SA for the particles prepared by the addition of a smaller initial amount of SA (Ch:SA (1:0.5)) was not as clearly observed (Fig. 5d), which could imply that all the SA is encapsulated by the chitosan when a low content of SA is added.

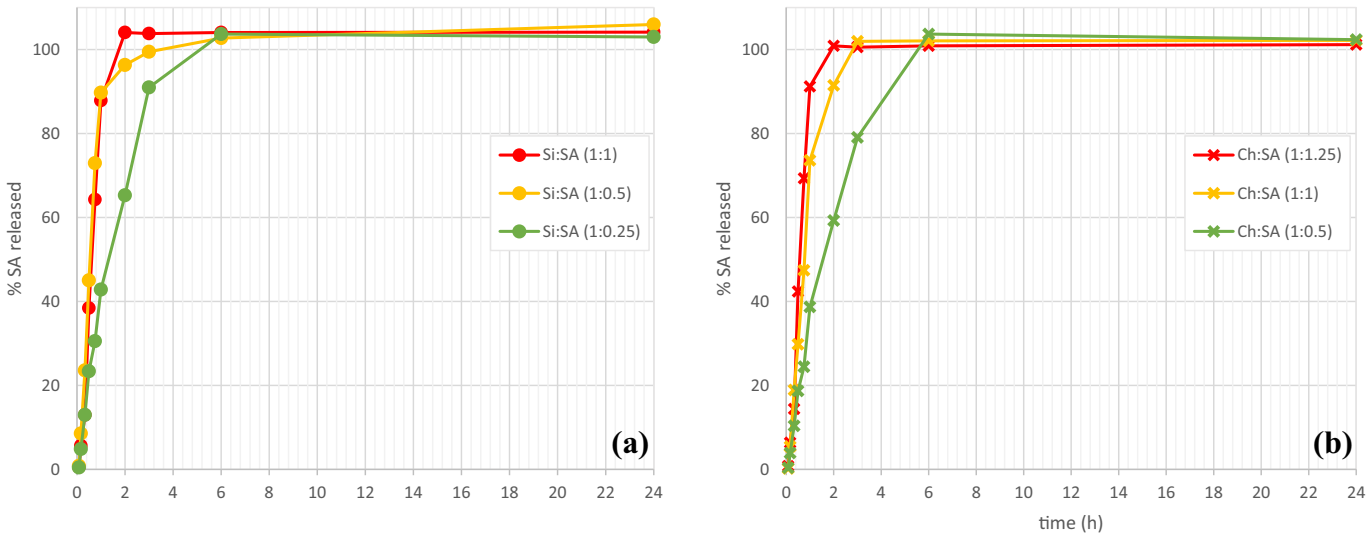

Fig. 8. SA release from encapsulated samples prepared with silica (a) and chitosan (b) for the three capsule:SA studied ratios.

3.1.4. SEM-EDX

Semi-quantitative Energy Dispersive X-ray (EDX) microanalysis of SA encapsulated in silica (Si:SA) and chitosan (Ch:SA) are depicted in Figs. 6 and 7, respectively, together with the SEM micrographs analysed in each case.

SEM/EDX results of the encapsulated samples with silica (Si:SA) (Fig. 6) revealed the presence of three main components: carbon, oxygen and silicon. While oxygen is present in both capsule and encapsulated, carbon can only be found in the SA molecule, and silicon in the silica one, which facilitates the SEM/EDX results interpretation. SA can be easily identified on the surface of the spherical particles, both visually and analytically. Visually by comparing the "Dark" SEM micrograph with the "Light" one and, analytically, by the higher carbon content detected by SEM/EDX analysis on the surface of the loaded silica particles ("Dark" and "Outer" in Fig. 6), which can be only associated to the SA molecule. "Inner" SEM/EDX analysis (corresponding to the interior of a loaded silica particle) revealed a decrease in carbon content and an increase in silicon, what may be due to a gradual distribution of SA from the outside to the inside of the spherical silica particles.

SEM/EDX results of the encapsulated samples with chitosan (Ch:SA) (Fig. 7) revealed the presence of five main components: carbon, oxygen, nitrogen, phosphorous and sodium. In this case, carbon and oxygen are present in both capsule and encapsulated, leaving as differential elements the nitrogen, assigned to chitosan molecule, and the phosphorous and the sodium, which correspond to the TPP-Na cross-linking material. The lack of a distinguishing chemical element between capsule and encapsulated makes the interpretation of the SEM/EDX results much more difficult with respect to the previous silica samples. However, an unusual kind of particle with a smoother surface was detected (marked as 1 in Fig. 7), since most of the observed particles were similar to those identified as 2 to 5 in Fig. 7. This isolate particle has a different chemical composition with lower contents of nitrogen, phosphorus and sodium, which suggest that it could correspond to free SA that have not been adequately encapsulated by chitosan during the process. SEM/EDX analysis of the 2 to 5 marked particles revealed a higher content of nitrogen, phosphorus and sodium, which should correspond to the TPP-Na crosslinked chitosan (capsule material). Indeed, as have been suggested by other authors [33,39], high contents on phosphorus (and sodium in our case) can be related to a worst encapsulation process, since a complete entrapment of the SA within the chitosan particles would probably not leave enough space for the TPP to cross-link with the chitosan chains, compared with the unloaded chitosan cross-linked particles. The higher cross-linking density of the unloaded particles would result in a higher phosphorus content (around 50% according to previous findings [33]). Hence, the low contents of P and Na identified in our samples (lower than 10%) were found to be in agreement with data reported in the literature [33], suggesting a good SA entrapment within chitosan particles.

Table 2
Mathematical values obtained from Korsmeyer-Peppas model. K, n and r^2 represents kinetic constant, release exponent and Pearson coefficient, respectively, of the encapsulated samples prepared with silica (Si:SA) and chitosan (Ch:SA).

SAMPLE	k (h^{-n})	n	r^2
Si:SA (1:1)	0.70	1.66	0.92
Si:SA (1:0.5)	0.59	1.26	0.83
Si:SA (1:0.25)	0.28	1.16	0.86
Ch:SA (1:1.25)	0.66	1.57	0.91
Ch:SA (1:1)	0.48	1.52	0.86
Ch:SA (1:0.5)	0.31	1.22	0.88

3.1.5. Encapsulation efficiency of SA

Encapsulation efficiency (EE%) results are shown in Table 1. The average EE% of the encapsulated SA with silica and chitosan were 61.9% and 46.7%, respectively, and in both cases the lowest EE% value corresponded to the lowest ratio studied (1:0.25 in the silica samples and 1:0.5 in the chitosan ones). The differences in EE% found between the two capsules could be explained by the different encapsulation process conducted in each case. During processing, the solid content of the samples with silica (Si:SA) was higher than those of chitosan (Ch:SA) (13.5% vs 3.6–2.8%), and the speed of the planetary mill used was lower (180 vs 210 rpm), which, as it was found, meant less wear of the grinding media; a fact that could explain the higher values of the encapsulation efficiency obtained. In the same vein, SA appears to be embedded in the porous structure of the silica capsule and entrapped within the polymer chains of chitosan and thereafter cross-linked with TPP-Na. Pure amorphous silica particles have a high specific surface area (117 m^2/g), which could allow a high loading of SA inside, and explain the higher EE% achieved with this capsule.

Contrary to what might be expected, the lowest ratios also resulted in the lowest EE% values, regardless of the capsule tested. The reason, as reported in literature, could be attribute to the capsule saturation [40]. Higher contents in SA could lead to capsule saturation and an increase of the free SA (unable to bind to saturated chitosan or to penetrate saturated silica), reducing the EE%.

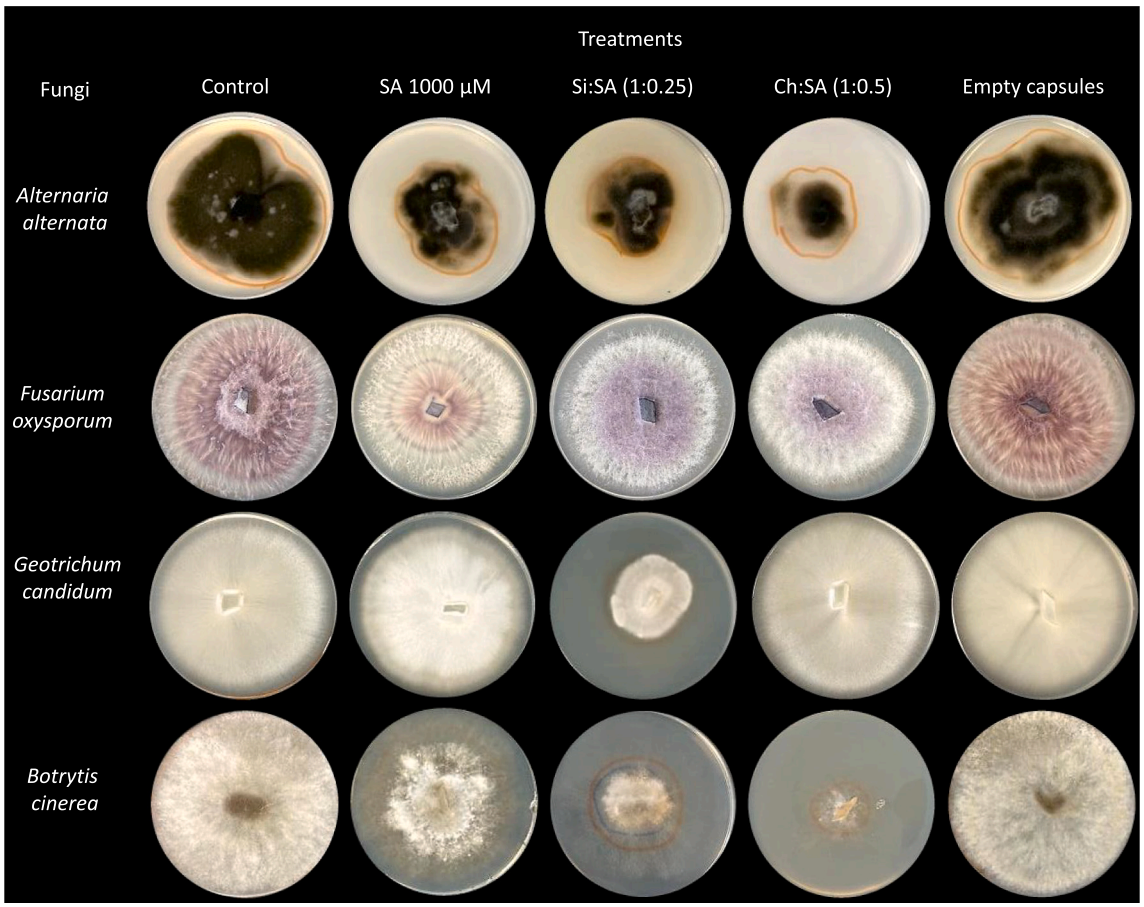

Fig. 9. Antifungal effects of Si:SA (1:0.25) and Ch:SA (1:0.5) capsules at 1000 μM. Last column represent capsules without salicylic acid. The others studied ratios are not in the figure because they did not have representative mycelial inhibition effect. *Phytophthora infestans* is not in the figure because neither of the three capsule:SA studied ratios had a representative growth inhibition effect on it at 1000 μM.

3.2. *In vitro kinetics of SA release*

Encapsulation systems were evaluated to determine their products kinetics and their release mechanism. In vitro cumulative release was performed on the three studied ratios of the encapsulated samples with silica (Si:SA) and chitosan (Ch:SA) (Fig. 8a and b, respectively). The magnetic stirring was kept at the lowest speed allowed by the equipment in order that the constant mechanical movement did not induce physical damage to the capsule and that the SA could be detached from it following a natural extraction process [41]. Results showed that SA was released in the first 6 h in a single stage (for both capsules and for the three ratios tested), and the results with chitosan being in agreement with precedent studies found in the literature [42].

The Korsmeyer-Peppas model, which has already been used to evaluate the release kinetics of another encapsulated phytohormones such as gibberellic acid [37], was used to determine the release mechanism and kinetics of SA from the two capsules studied. As mentioned before, the value of n in Eq. (3) determines the kind of release mechanism, that is Fickian or non-Fickian (anomalous) diffusion, while the k value in the same equation determines the speed of release [43].

The linear plot of $ln(M_t/M_\infty)$ versus $ln(t)$ yielded to the diffusion exponent (n), the regression values (r^2) and the diffusion constant (k) depicted in Table 2. Diffusion exponent (n) was found to be 1.16–1.66 for the encapsulated samples with silica (Si:SA) and 1.22–1.57 for those with chitosan (Ch:SA), what corresponds to a non-Fickian (case II transport) release mechanism, and which means that SA is released from silica and chitosan capsules by dissolution or relaxation of polymer chains within the capsule [44,45].

The value of k (Table 2) is positively correlated with the release rate kinetics [46]. The highest values of k were observed with the highest ratios tested, which indeed corresponded to the highest EE%. The increase of SA in the polymer matrix, which resulted in an increase of Ch-TPP nanogel hydrophilic character, seems to favour the release of the encapsulated hormone, as previously found in the literature [47]. During the swelling and relaxation process, the water embedded in the chitosan matrix untangles and loosens the polymer chains, providing greater mobility for the hormone and allowing it to diffuse from the polymer matrix to the surrounding medium [48]. This could be also explained by the hypothesis that the higher ratios could present a saturation of the capsules with a part of the SA not effectively encapsulated [40].

3.3. *Antifungal activity of Si:SA and Ch:SA samples*

As it is known, SA has antifungal effects as a decoupling agent of organelle membranes [49] and directly affects the fungal development in *Eutypa lata* by a displacement of the hydroxyl group on the aromatic ring of the SA structure [50], thus reducing the fungal growth. To test if the hormone has also toxic effects on different fungi of agronomical importance, a preliminary toxicity curve of SA with different concentrations was conducted on *A. alternata*, *F. oxysporum*, *G. candidum*, *P. infestans* and *B. cinerea* (see Supplementary Table 3 and Supplementary Fig. 2 and 3). *A. alternata* and *B. cinerea* inhibition rates were found to be 45.72 % and 42.11 %, respectively; both recorded at maximum SA concentration of 1000 μM. Inhibition rates for *F. oxysporum* and *G. candidum* were 19.83% and 21.27%, respectively, while *P. infestans* did not show mycelial inhibition at any concentration of SA. *A. alternata*

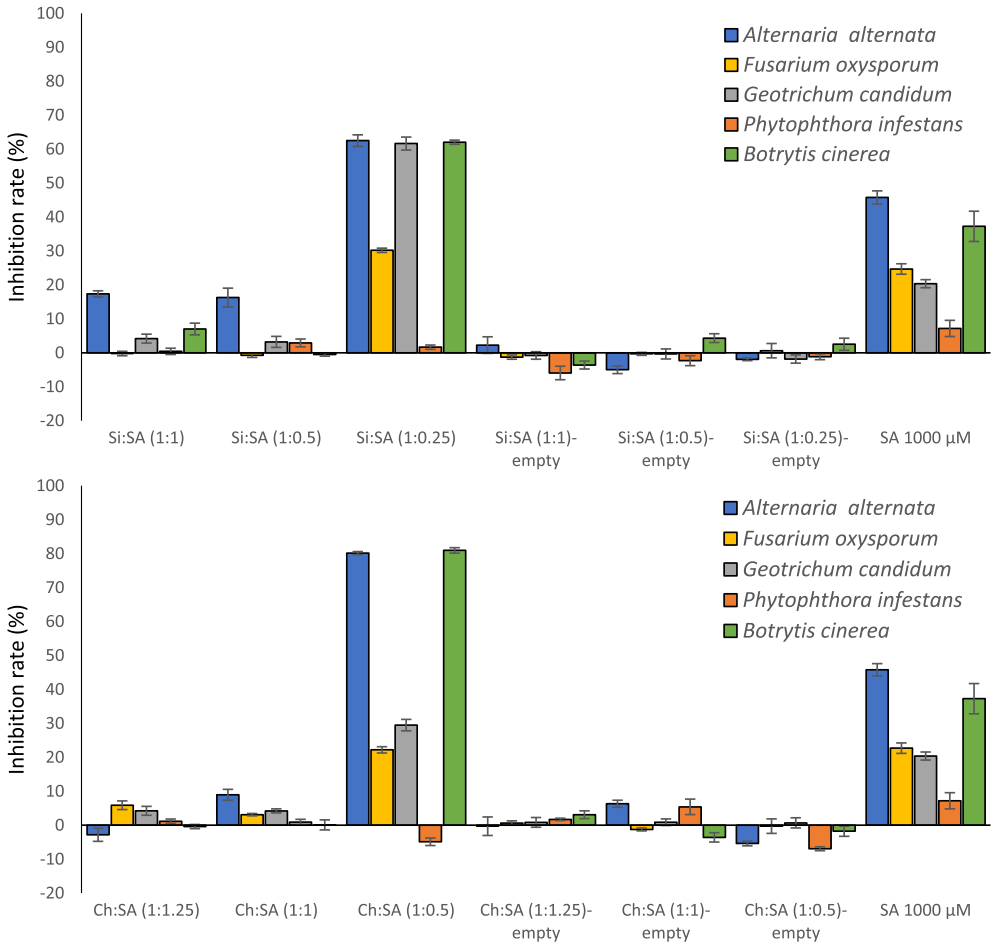

Fig. 10. Fungal inhibition rates of the encapsulated samples at 1000 µM. "Empty" samples correspond to capsules without SA. Results for *Alternaria alternata*, *Fusarium oxysporum*, *Geotrichum candidum*, *Phytophthora infestans* and *Botrytis cinerea* are shown in blue, yellow, grey, orange and green, respectively.

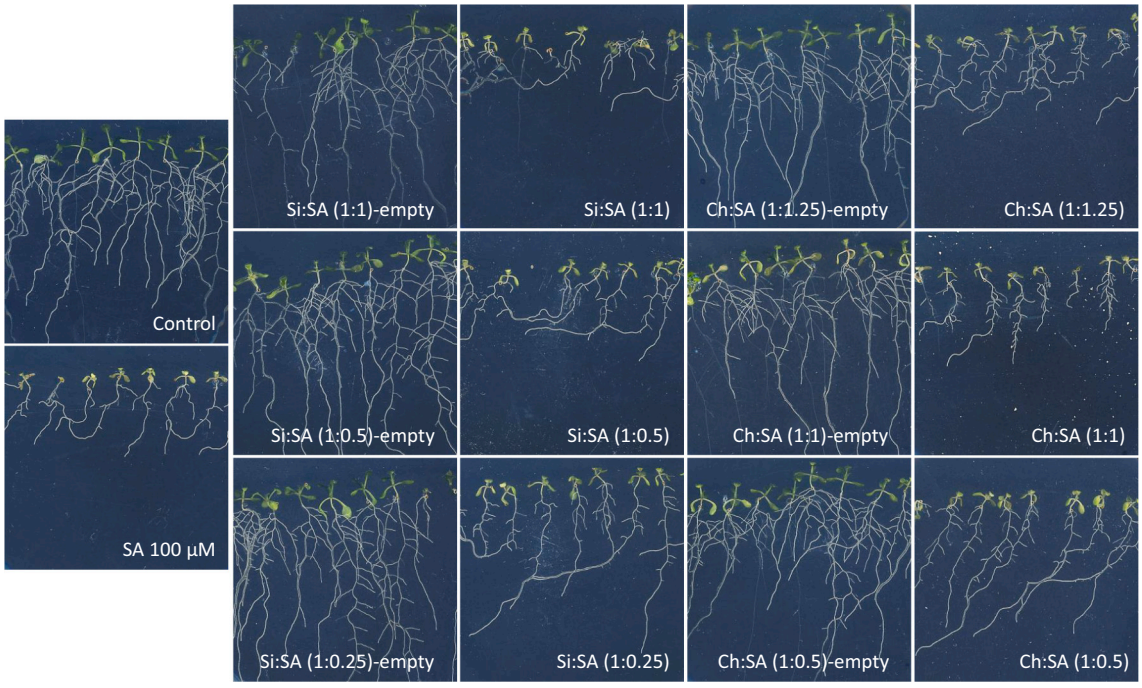

Fig. 11. Effect of the encapsulated samples at 100 µM on the growth and development of *Arabidopsis thaliana* plants (12 days after seeds sowed). "Empty" samples correspond to capsules without salicylic acid (SA).

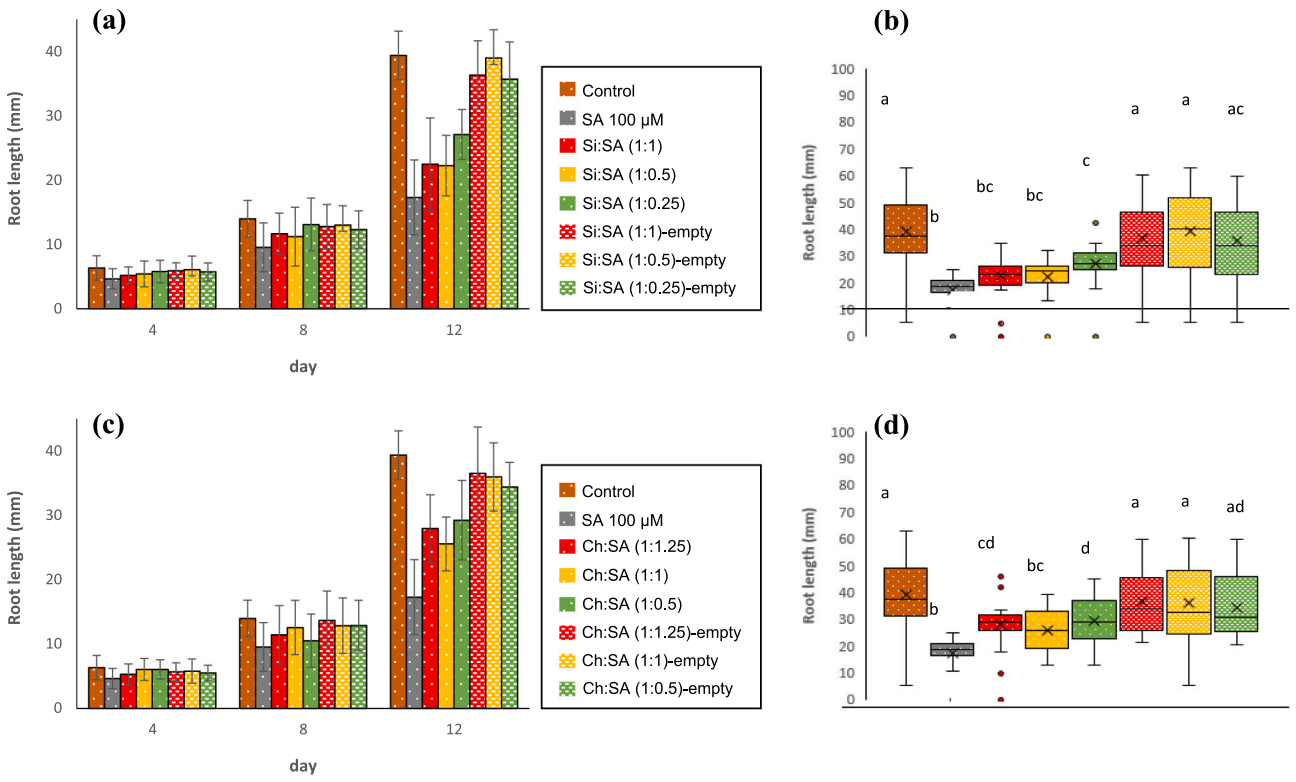

Fig. 12. Root length quantification of the encapsulated samples at 100 μM. *Arabidopsis thaliana* plants at 4, 8 and 12 days after seeds sowed for the encapsulated samples prepared with silica (a) and chitosan (c) and box plot at 12 days after seeds sowed for the encapsulated samples prepared with silica (b) and chitosan (d). "Empty" samples correspond to capsules without salicylic acid (SA).

and *B. cinerea* showed mycelial inhibition between 100 and 1000 μM SA concentration, and *F. oxysporum* and *G. candidum* in the 700–1000 μM range. In view of these results, 100, 500 and 1000 μM SA concentrations were selected to test the encapsulated samples with silica (Si:SA) and chitosan (Ch:SA).

Supplementary Table 4 and Supplementary Fig. 4 and 5 depict the results obtained for 100 μM treatments. As can be seen, the empty capsules did not have any antifungal effect on their own at the tested concentrations. Mycelial growth of *A. alternata* and *B. cinerea* was reduced by 100 μM SA, with inhibition rates of 16.5% and 11.6%, respectively, while Si:SA (1:0.25) and Ch:SA (1:0.5) caused inhibition rates of 34.1% and 43.1% for *A. alternata* and 17.3% and 38.8% for *B. cinerea*, respectively. These values exceed the *A. alternata* and *B. cinerea* inhibition rates caused by the free hormone, which means that encapsulation increased antifungal activity and that the capsules act only as carriers, since they have no effect on fungi by themselves. The ratios at 100 μM did not affect the mycelial growth of *A. alternata* and *B. cinerea* (see Supplementary Table 4 and Supplementary Fig. 5). In the case of *F. oxysporum*, *G. candidum* and *P. infestans*, none of the three capsule:SA ratios at 100 μM affected the mycelial growth of the fungi (see Supplementary Table 4 and Supplementary Fig. 5).

In the same way, Supplementary Table 4 and Supplementary Fig. 6 and 7 depict the results obtained for 500 μM treatments. The radial growth of *A. alternata* and *B. cinerea* was highly decreased related to control, with inhibition rates of 30.8% and 20.4% rates, respectively. Treatments with Si:SA (1:0.25) and Ch:SA (1:0.5) at 500 μM caused higher inhibition rates of 52.8% and 55.9% for *A. alternata* and of 31.9% and 57.1% for *B. cinerea*, respectively. Inhibition rate for *F. oxysporum* was of the 16.4 % with the 500 μM SA concentration and 22.9% for the Si:SA (1:0.25) treatment. As can be seen in the Supplementary Table 4 and the Supplementary Fig. 7, the ratios at 500 μM did not affect the mycelial growth of *A. alternata*, *B. cinerea* and *F. oxysporum*, and in the case of *G. candidum* and *P. infestans*, neither of the three ratios studied affect their mycelial growth.

At 1000 μM (see Supplementary Table 4 and Figs. 9 and 10), Si:SA (1:0.25) and Ch:SA (1:0.5) treatments displayed a strong inhibition rate for *A. alternata* (62.5% and 80.1%, respectively) and *B. cinerea* (62.0% and 80.9%, respectively). The inhibition rates values for *F. oxysporum* were 30.2% with the Si:SA (1:0.25) treatment and 22.2% with the Ch:SA (1:0.5) one. Mycelial growth inhibition rate for *G. candidum* was 61.6% and 29.5% with Si:SA (1:0.25) and Ch:SA (1:0.5), respectively. It may be notice that these values were higher than those obtained with the 1000 μM SA concentration (45.8%, 37,3%, 24,7% and 20,4%, corresponding to *A. alternata*, *B. cinerea*, *F. oxysporum* and *G. candidum,* respectively). In general, the radial growth of fungi was reduced to a greater extent with the smallest ratio treatments of both samples (Si:SA and Ch:SA), which could be explained by the maximum content of SA within each capsule. Due to the porous nature of the amorphous silica, SA could oversaturate its internal surface through the formation of an agglutinate, preventing the correct release of SA in the highest Si:SA ratios [51]. On the other hand, and high content of SA could hinder the correct formation of links between chitosan and TPP-Na, giving rise to an unstable structure with an ineffective SA release. Furthermore, as observed in the kinetics analysis, samples with lower ratios of SA release it in a more controlled way, affecting fungal growth for longer than free SA. In summary, the encapsulation process with both capsules (silica or chitosan) increases the antifungal activity of SA, being the samples with the lowest ratios of SA the ones that provide the best results.

3.4. Effect of Si:SA and Ch:SA samples on Arabidopsis root growth

The effect of Si:SA and Ch:SA treatments on plant development was evaluated with three doses (100, 500 and 1000 μM) to determine the maximum SA concentration that Arabidopsis plants can tolerate without conditioning their growth. The results (see Supplementary Fig. 8) showed an intense inhibition growth at the concentrations of 500 and

1000 μM. A totally inhibited-germination of Arabidopsis seeds was observed at SA 1000 μM, probably because SA is playing a negative regulator role, inducing oxidative stress [52,53]. In the case of 100 μM SA treatment, although the inhibition was much lighter, a lower development of the roots and aerial parts was also observed compared to the controls.

From preliminary results, 100 μM was the chosen dose for further experiments. Figs. 11 and 12 show that treatments with the lowest contents of SA (1:0.25 for Si:SA and 1:0.5 for Ch:SA), which were more effective in increasing Arabidopsis roots length compared to those treated with free SA (see Fig. 12a-c). The day 12 after sowing, roots treated with Si:SA (1:0.25) and Ch:SA (1:0.5) at 100 μM had a growth of 27.1 mm and 29.2 mm, respectively. In contrast, treatment with free SA leaded to a root growth of 17.3 mm (see Fig. 12b-d). Therefore, it can be concluded that encapsulation reverses the toxic effect of free SA.

In Arabidopsis, SA plays a central role in the regulation of several plant functions and induces antioxidant defences in abiotic or biotic stress [54]. Nevertheless, over accumulation of SA induces a programmed cell death. During stress, there is a trade-off between resistance and growth and SA endogenous accumulation triggers the immune responses that allow survival but penalize growth [55]. Treatments with exogenous SA reduce in a dose-dependent manner the Arabidopsis root elongation, inhibiting cell proliferation. Moreover, high-dosage of SA inhibits cell cycle progression and induces the auxin accumulation that inhibits lateral root development [56].

Encapsulation of SA to lower ratios is highly effective because it allows a controlled SA release. As aforementioned, this could be explained by the differences in kinetics release since lower values of the kinetic constant (k) allow a slower release of SA, reducing the amount of SA available in the medium (susceptible to be absorbed by the plant) and decreasing its over accumulation and its toxicity. Samples with higher ratios (1:0.5 and 1:1 for Si:SA and 1:1 and 1:1.25 for Ch:SA), as well as the free SA, gave worse results since, as mentioned above, these samples seem to lead to less effective encapsulations, having, in the case of silica capsules, an excess of SA on the surface, and in the case of chitosan, a poor encapsulation, being this excess of free SA the cause of the increased toxicity in plant cells [57]. It should be also noticed that the capsules per se did not show any significant effect on Arabidopsis root growth.

It is also important to note that the conditions tested, both in anti-pathogenic activity and in plant growth, are extreme conditions, far from the real scenario of the cultivation fields. The doses of the treatments tested should therefore be adjusted to this real scenario and optimized according to the nature of the crop.

4. Conclusions

Encapsulated systems for the SA phytohormone with silica or chitosan as carriers were successfully prepared by spray drying, which is an easily scalable industrial manufacturing process, and their physicochemical characteristics and biological effects studied. The lowest capsule:SA ratios provided a good controlled release of the phytohormone, better than the others ratios studied because a smaller amount of SA could be encapsulated more efficiently without saturating the capsule. In vitro assays against *A. alternata, B. cinerea, F. oxysporum,* and *G. candidum* of Si:SA (1:0.25) and Ch:SA (1:0.5) treatments were found to have a stronger inhibition effect in mycelial growth than free SA, since a slow SA release affects effectively for longer times. Necrotrophic and biotrophic fungi attack around 200 crops worldwide, causing water-soaking of tissues and the subsequent appearance of grey masses on leaves, stems and fruits [58], difficult to control with fungicides due to their genetic plasticity [59]. For this reason, encapsulated samples are a great alternative for anti-fungal activity control, being able to be tested in vitro and *in vivo*, as well as in others pathogenic fungi. Moreover, the efficacy of the treatments allows carrying out new studies to formulate new active fungicide for crop protection.

Similarly, in biological assays of Arabidopsis seeds, the lowest ratios samples studied of both carriers (silica and chitosan), reversed the toxic effect on the development of plant growth by reducing the over-accumulation of free SA in the medium. The effect on plants of the higher ratios samples and free SA was considerable worse, avoiding the correct formation and growing of roots and rosettes. These results can be extrapolated to biotic and abiotic stress assays in plants where a particular PGRs can have enhanced effects, giving to the plant the capacity to tolerate and/or mitigate stress damage. Finally, the use of capsule systems for any PGRs can enhance its biological activity and efficiency when used in the field, resulting in an agricultural product with a higher quality and important economic value.

CRediT authorship contribution statement

Design, conceptualization: Sampedro-Guerrero, J.; Vives-Peris, V.; Gomez-Cadenas, A; Clausell-Terol, C.; manuscript writing and proof-reading: Sampedro-Guerrero, J.; Gomez-Cadenas, A; Clausell-Terol, C.; experimental work, data analysis, and interpretation: Sampedro-Guerrero, J.; Vives-Peris, V.; Gomez-Cadenas, A; Clausell-Terol, C. All authors have read and agreed to the published version of the manuscript.

Declaration of Competing Interest

The authors declare that they have no known competing financial interests or personal relationships that could have appeared to influence the work reported in this paper.

Acknowledgement

This work was supported by MCIN/AEI/10.13039/501100011033 through grant PID2019-104062RB-I00 and Universitat Jaume I through grants UJI-B2019-11 and UJI-B2020-13. JS-G was hired through the Santiago Grisolia program of Generalitat Valenciana (GRISOLIAP/2020/043).

Appendix A. Supplementary material

Supplementary data to this article can be found online at https://doi.org/10.1016/j.ijbiomac.2021.12.124.

References

[1] A. Gharsallaoui, G. Roudaut, O. Chambin, A. Voilley, R. Saurel, Applications of spray-drying in microencapsulation of food ingredients: An overview, Food Res. Int. 40 (9) (2007) 1107–1121, https://doi.org/10.1016/j.foodres.2007.07.004.
[2] D. Gunther, Ö. Bilal, Z. Wenjun, S. Amir, H. Joseph, H.B. J., Plant Pathogenic Fungi, Microbiol. Spectr. 5 (2017) 5.1.14. https://doi.org/10.1128/microbiolspec.FUNK-0023-2016.
[3] Y.M. Koo, A.Y. Heo, H.W. Choi, Salicylic Acid as a Safe Plant Protector and Growth Regulator, Plant Pathol. J. 36 (1) (2020) 1–10, https://doi.org/10.5423/PPJ.RW.12.2019.0295.
[4] W. Rademacher, Plant Growth Regulators: Backgrounds and Uses in Plant Production, J. Plant Growth Regul. 34 (4) (2015) 845–872, https://doi.org/10.1007/s00344-015-9541-6.
[5] C.C. Small, D. Degenhardt, Plant growth regulators for enhancing revegetation success in reclamation: A review, Ecol. Eng. 118 (2018) 43–51. https://doi.org/https://doi.org/10.1016/j.ecoleng.2018.04.010.
[6] J.P. Tadeu Dias, Plant growth regulators in horticulture: practices and perspectives, Biotecnol. Veg. 19 (2019) 03–14.
[7] D.A. Dempsey, D.F. Klessig, How does the multifaceted plant hormone salicylic acid combat disease in plants and are similar mechanisms utilized in humans? BMC Biol. 15 (2017) 23, https://doi.org/10.1186/s12915-017-0364-8.
[8] T. Janda, G. Szalai, M. Pál, Salicylic acid signalling in plants, Int. J. Mol. Sci. 21 (7) (2020) 2655, https://doi.org/10.3390/ijms21072655.
[9] V. Saharan, A. Mehrotra, R. Khatik, P. Rawal, S.S. Sharma, A. Pal, Synthesis of chitosan based nanoparticles and their in vitro evaluation against phytopathogenic fungi, Int. J. Biol. Macromol. 62 (2013) 677–683, https://doi.org/10.1016/j.ijbiomac.2013.10.012.
[10] K. Miura, Y. Tada, Regulation of water, salinity, and cold stress responses by salicylic acid, Front. Plant Sci. 5 (2014) 4.

[11] M.I.R. Khan, M. Fatma, T.S. Per, N.A. Anjum, N.A. Khan, Salicylic acid-induced abiotic stress tolerance and underlying mechanisms in plants, Front. Plant Sci. 6 (2015) 462.
[12] A. Alonso-Ramírez, D. Rodríguez, D. Reyes, J.A. Jiménez, G. Nicolás, M. López-Climent, A. Gómez-Cadenas, C. Nicolás, Evidence for a Role of Gibberellins in Salicylic Acid-Modulated Early Plant Responses to Abiotic Stress in Arabidopsis Seeds, Plant Physiol. 150 (3) (2009) 1335–1344, https://doi.org/10.1104/pp.109.139352.
[13] K. Vlahoviček-Kahlina, S. Jurić, M. Marijan, B. Mutaliyeva, S.V. Khalus, A. V. Prosyanik, M. Vinceković, Synthesis, Characterization, and Encapsulation of Novel Plant Growth Regulators (PGRs) in Biopolymer Matrices, Int. J. Mol. Sci. 22 (4) (2021) 1847, https://doi.org/10.3390/ijms22041847.
[14] R. Prasad, A. Bhattacharyya, Q.D. Nguyen, Nanotechnology in Sustainable Agriculture: Recent Developments, Challenges, and Perspectives, Front. Microbiol. 8 (2017) 1014, https://doi.org/10.3389/fmicb.2017.01014.
[15] P.N. Ezhilarasi, P. Karthik, N. Chhanwal, C. Anandharamakrishnan, Nanoencapsulation Techniques for Food Bioactive Components: A Review, Food Bioprocess Technol. 6 (3) (2013) 628–647, https://doi.org/10.1007/s11947-012-0944-0.
[16] R. Becerril, C. Nerín, F. Silva, Encapsulation Systems for Antimicrobial Food Packaging Components: An Update, Mol. 25 (5) (2020) 1134, https://doi.org/10.3390/molecules25051134.
[17] L.F. Fraceto, R. Grillo, G.A. de Medeiros, V. Scognamiglio, G. Rea, C. Bartolucci, Nanotechnology in Agriculture: Which Innovation Potential Does It Have? Front. Environ. Sci. 4 (2016) 20.
[18] A. Mohan, S.R.C.K. Rajendran, Q.S. He, L. Bazinet, C.C. Udenigwe, Encapsulation of food protein hydrolysates and peptides: a review, RSC Adv. 5 (97) (2015) 79270–79278, https://doi.org/10.1039/C5RA13419F.
[19] Z.A. Raza, S. Khalil, A. Ayub, I.M. Banat, Recent developments in chitosan encapsulation of various active ingredients for multifunctional applications, Carbohydr. Res. 492 (2020) 108004. https://doi.org/https://doi.org/10.1016/j.carres.2020.108004.
[20] D. Wibowo, Y. Hui, A.P.J. Middelberg, C.-X. Zhao, Interfacial engineering for silica nanocapsules, Adv. Colloid Interface Sci. 236 (2016) 83–100. https://doi.org/https://doi.org/10.1016/j.cis.2016.08.001.
[21] A.B. Seabra, M. Rai, N. Durán, Nano carriers for nitric oxide delivery and its potential applications in plant physiological process : A mini review 23 (2014) 1–10, https://doi.org/10.1007/s13562-013-0204-z.
[22] D. Mittal, G. Kaur, P. Singh, K. Yadav, S.A. Ali, Nanoparticle-Based Sustainable Agriculture and Food Science: Recent Advances and Future Outlook, Front. Nanotechnol. 2 (2020) 10.
[23] R.W. Korsmeyer, R. Gurny, E. Doelker, P. Buri, N.A. Peppas, Mechanisms of solute release from porous hydrophilic polymers, Int. J. Pharm. 15 (1) (1983) 25–35, https://doi.org/10.1016/0378-5173(83)90064-9.
[24] T. Murashige, F. Skoog, A revised medium for rapid growth and bio assays with tobacco tissue cultures, Physiol. Plant. 15 (3) (1962) 473–497.
[25] I. Betegón-Putze, A. González, X. Sevillano, D. Blasco-Escámez, A.I. Caño-Delgado, MyROOT: a method and software for the semiautomatic measurement of primary root length in Arabidopsis seedlings, Plant J. 98 (2019) 1145–1156, https://doi.org/10.1111/tpj.14297.
[26] W.J. Walker, J.S. Reed, S.K. Verma, Influence of slurry parameters on the characteristics of spray-dried granules, J. Am. Ceram. Soc. 82 (1999) 1711–1719, https://doi.org/10.1111/j.1151-2916.1999.tb01990.x.
[27] K. Mohanta, P. Bhargava, Effect of milling time on the rheology of highly loaded aqueous-fused silica slurry, J. Am. Ceram. Soc. 91 (2) (2008) 640–643, https://doi.org/10.1111/j.1551-2916.2007.02153.x.
[28] P.K. Mishra, B.B. Nayak, B.K. Mishra, Influence of behaviour of alumina slurry on quality of alumina powder prepared by jet wheel impact atomization, Powder Technol. 196 (3) (2009) 272–277, https://doi.org/10.1016/j.powtec.2009.08.013.
[29] P. Höhne, B. Mieller, T. Rabe, Slurry development for spray granulation of ceramic multicomponent batches, J. Ceram. Sci. Technol. 9 (2018) 327–336, https://doi.org/10.4416/JCST2018-00022.
[30] P.-C. Lin, S. Lin, P.C. Wang, R. Sridhar, Techniques for physicochemical characterization of nanomaterials, Biotechnol. Adv. 32 (4) (2014) 711–726, https://doi.org/10.1016/j.biotechadv.2013.11.006.
[31] M.A. Ashraf, A.M. Khan, M. Sarfraz, M. Ahmad, Effectiveness of silica based sol-gel microencapsulation method for odorants and flavors leading to sustainable environment , Front. Chem. . 3 (2015) 42. https://www.frontiersin.org/article/10.3389/fchem.2015.00042.
[32] I. Silvestro, I. Francolini, V. Di Lisio, A. Martinelli, L. Pietrelli, A. Scotto d'Abusco, A. Scoppio, A. Piozzi, Preparation and characterization of TPP-chitosan crosslinked scaffolds for tissue engineering, Materials (Basel). 13 (16) (2020) 3577.
[33] A. Shetta, J. Kegere, W. Mamdouh, Comparative study of encapsulated peppermint and green tea essential oils in chitosan nanoparticles: Encapsulation, thermal stability, in-vitro release, antioxidant and antibacterial activities, Int. J. Biol. Macromol. 126 (2019) 731–742, https://doi.org/10.1016/j.ijbiomac.2018.12.161.
[34] S. Sharifi, S. Behzadi, S. Laurent, M. Laird Forrest, P. Stroeve, M. Mahmoudi, Toxicity of nanomaterials, Chem. Soc. Rev. 41 (6) (2012) 2323–2343.
[35] A. Sukhanova, S. Bozrova, P. Sokolov, M. Berestovoy, A. Karaulov, I. Nabiev, Dependence of Nanoparticle Toxicity on Their Physical and Chemical Properties, Nanoscale Res. Lett. 13 (2018) 44, https://doi.org/10.1186/s11671-018-2457-x.
[36] J.A. Gallego-Urrea, J. Tuoriniemi, M. Hassellöv, Applications of particle-tracking analysis to the determination of size distributions and concentrations of nanoparticles in environmental, biological and food samples, TrAC Trends Anal. Chem. 30 (2011) 473–483. https://doi.org/https://doi.org/10.1016/j.trac.2011.01.005.
[37] A.E.S. Pereira, P.M. Silva, J.L. Oliveira, H.C. Oliveira, L.F. Fraceto, Chitosan nanoparticles as carrier systems for the plant growth hormone gibberellic acid, Colloids Surfaces B Biointerfaces. 150 (2017) 141–152, https://doi.org/10.1016/j.colsurfb.2016.11.027.
[38] L. Keawchaoon, R. Yoksan, Preparation, characterization and in vitro release study of carvacrol-loaded chitosan nanoparticles, Colloids Surfaces B Biointerfaces. 84 (1) (2011) 163–171, https://doi.org/10.1016/j.colsurfb.2010.12.031.
[39] D.R. Bhumkar, V.B. Pokharkar, Studies on effect of pH on cross-linking of Chitosan with sodium tripolyphosphate: A technical note, AAPS PharmSciTech. 7 (2) (2006) E138–E143, https://doi.org/10.1208/pt070250.
[40] C.P. Oliveira, C.G. Venturini, B. Donida, F.S. Poletto, S.S. Guterres, A.R. Pohlmann, An algorithm to determine the mechanism of drug distribution in lipid-core nanocapsule formulations, Soft Matter 9 (4) (2013) 1141–1150, https://doi.org/10.1039/C2SM26959G.
[41] S. Klein, Influence of different test parameters on in vitro drug release from topical diclofenac formulations in a vertical diffusion cell setup, Pharmazie. 68 (2013) 565–571, https://doi.org/10.1691/ph.2013.6528.
[42] Z. Yang, Y. Fang, H. Ji, Controlled release and enhanced antibacterial activity of salicylic acid by hydrogen bonding with chitosan, Chinese, J Chem. Eng. 24 (3) (2016) 421–426, https://doi.org/10.1016/j.cjche.2015.08.008.
[43] I.Y. Wu, S. Bala, N. Škalko-Basnet, M.P. di Cagno, Interpreting non-linear drug diffusion data: Utilizing Korsmeyer-Peppas model to study drug release from liposomes, Eur. J. Pharm. Sci. 138 (2019) 105026. https://doi.org/https://doi.org/10.1016/j.ejps.2019.105026.
[44] A.K. Nayak, D. Pal, Formulation optimization and evaluation of jackfruit seed starch–alginate mucoadhesive beads of metformin HCl, Int. J. Biol. Macromol. 59 (2013) 264–272. https://doi.org/https://doi.org/10.1016/j.ijbiomac.2013.04.062.
[45] T. Maver, T. Mohan, L. Gradišnik, M. Finšgar, K. Stana Kleinschek, U. Maver, Polysaccharide Thin Solid Films for Analgesic Drug Delivery and Growth of Human Skin Cells, Front. Chem. 7 (2019) 217, https://doi.org/10.3389/fchem.2019.00217.
[46] K.I. Matshetshe, S. Parani, S.M. Manki, O.S. Oluwafemi, Preparation, characterization and in vitro release study of β-cyclodextrin/chitosan nanoparticles loaded Cinnamomum zeylanicum essential oil, Int. J. Biol. Macromol. 118 (2018) 676–682, https://doi.org/10.1016/j.ijbiomac.2018.06.125.
[47] F.O.M.S. Abreu, E.F. Oliveira, H.C.B. Paula, R.C.M. de Paula, Chitosan/cashew gum nanogels for essential oil encapsulation, Carbohydr. Polym. 89 (4) (2012) 1277–1282, https://doi.org/10.1016/j.carbpol.2012.04.048.
[48] S.X. Tiew, M. Misran, Encapsulation of salicylic acid in acylated low molecular weight chitosan for sustained release topical application, J. Appl. Polym. Sci. 134 (2017) 1–11, https://doi.org/10.1002/app.45273.
[49] A.C. da Rocha Neto, M. Maraschin, R.M. Di Piero, Antifungal activity of salicylic acid against Penicillium expansum and its possible mechanisms of action, Int. J. Food Microbiol. 215 (2015) 64–70, https://doi.org/10.1016/j.ijfoodmicro.2015.08.018.
[50] B.-E. Amborabé, P. Fleurat-Lessard, J.-F. Chollet, G. Roblin, Antifungal effects of salicylic acid and other benzoic acid derivatives towards Eutypa lata: Structure-activity relationship, Plant Physiol. Biochem. 40 (12) (2002) 1051–1060, https://doi.org/10.1016/S0981-9428(02)01470-5.
[51] C. Mayer, Nanocapsules as drug delivery systems, Int. J. Artif. Organs. 28 (11) (2005) 1163–1171, https://doi.org/10.1177/039139880502801114.
[52] L. Rajjou, M. Belghazi, R. Huguet, C. Robin, A. Moreau, C. Job, D. Job, Proteomic Investigation of the Effect of Salicylic Acid on Arabidopsis Seed Germination and Establishment of Early Defense Mechanisms, Plant Physiol. 141 (2006) 910–923, https://doi.org/10.1104/pp.106.082057.
[53] M. Rivas-San Vicente, J. Plasencia, Salicylic acid beyond defence: its role in plant growth and development, J. Exp. Bot. 62 (10) (2011) 3321–3338, https://doi.org/10.1093/jxb/err031.
[54] N. Denancé, A. Sánchez-Vallet, D. Goffner, A. Molina, Disease resistance or growth: the role of plant hormones in balancing immune responses and fitness costs, Front. Plant Sci. 4 (2013) 155. https://www.frontiersin.org/article/10.3389/fpls.2013.00155.
[55] X. Han, R. Kahmann, Manipulation of Phytohormone Pathways by Effectors of Filamentous Plant Pathogens , Front. Plant Sci. . 10 (2019) 822. https://www.frontiersin.org/article/10.3389/fpls.2019.00822.
[56] T. Pasternak, E.P. Groot, F.V. Kazantsev, W. Teale, N. Omelyanchuk, V. Kovrizhnykh, K. Palme, V.V. Mironova, Salicylic Acid Affects Root Meristem Patterning via Auxin Distribution in a Concentration-Dependent Manner, Plant Physiol. 180 (3) (2019) 1725–1739, https://doi.org/10.1104/pp.19.00130.
[57] R.V. Kumaraswamy, S. Kumari, R.C. Choudhary, S.S. Sharma, A. Pal, R. Raliya, P. Biswas, V. Saharan, Salicylic acid functionalized chitosan nanoparticle: A sustainable biostimulant for plant, Int. J. Biol. Macromol. 123 (2019) 59–69, https://doi.org/10.1016/j.ijbiomac.2018.10.202.
[58] B. Williamson, B. Tudzynski, P. Tudzynski, J.A.L. Van Kan, Botrytis cinerea: The cause of grey mould disease, Mol. Plant Pathol. 8 (2007) 561–580. https://doi.org/10.1111/j.1364-3703.2007.00417.x.
[59] D. Shao, D.L. Smith, M. Kabbage, M.G. Roth, Effectors of Plant Necrotrophic Fungi, Front. Plant Sci. 12 (2021) 995.